L_1 adaptive controller design for a tail fin controlled fixed wing unmanned aerial vehicle

Alican Demirli[1,2], İlker Murat Koç[2], Burak Kürkçü[3]

[1] Aselsan INC., Yenimahalle, Ankara, Turkey
[2] Department of Mechanical Engineering, Istanbul Technical University, Istanbul, Turkey
[3] Mechanical System Control Laboratory, UC Berkeley, CA, USA

E-mail: demirlia@itu.edu.tr

Abstract. The aim of this study is to design L_1 adaptive controller, which is one of the robust control methods that can overcome model uncertainties, disturbances and noises, for a fixed-wing unmanned aerial vehicle (UAV) with tail fin controlled. In this context, first of all, the decoupled equations of motion of the six-degrees-of-freedom system are derived for the roll, pitch and yaw channels of the UAV. Then, the performance of the controller is demonstrated by simulation results for linearized system representation. By adding parameter errors to the system in question, the feature of tracking the given angle commands are analyzed. It has been observed that the L_1 adaptive control structure exhibits rapid adaptation even in presence of system uncertainties. Finally, the controller is applied to the nonlinear system and operated throughout the entire flight envelope.

1. Introduction

An unmanned aerial vehicle (UAV) is an aircraft beyond any human driver or passenger on board and they can be remotely controlled, flown partially autonomously, or flown autonomously [1]. The dynamics of a UAV constantly change during the flight of the UAV. The relatively small structure of UAVs makes them difficult to control under disturbances such as wind and noises such as sensor noise, and the systems may become unstable [2]. In addition, unmodeled system dynamics can also destabilize the UAV. For all these reasons, a robust control structure design that will keep the UAV stable during its flight becomes essential. To do it, various autopilot strategies providing stable flight for large flight envelope are proposed including a gain scheduled autopilot design [3], an adaptive autopilot design [4], $\mathcal{H}_\infty$ based switching control strategy [5] and model predictive control for attitude tracking [6].

Another remarkable design strategy for a flight control system is L_1 adaptive control. In this study, we present a complete guideline for L_1 adaptive control to validate the method for a no-thrust UAV system. The theoretical results are successfully implemented in a full-order nonlinear model considering uncertainties and disturbances. The results reveal good tracking performance as well as satisfying robust stability for a large flight envelope.

2. The UAV model

The system considered within the scope of the study is a six-degree-of-freedom UAV model. The system model with four tail fins and two fixed wings is given in figure 1. In the system studied,

there is no thrust force and the vehicle continues its motion with the energy of the moment it was thrown from the platform.

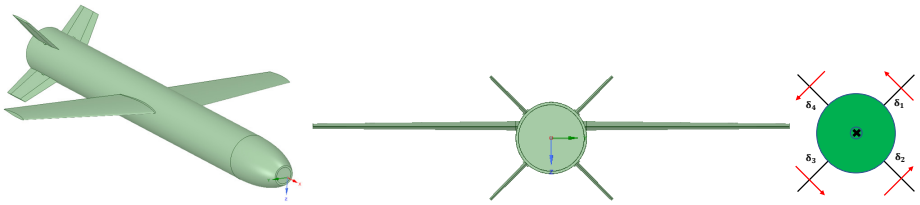

(a) The UAV model (b) The tail fins of the UAV

Figure 1: The UAV system

2.1. Equations of Motion (EOM)

In this section, 6-Degrees-of-Freedom (DOF) EOM are derived. The system in question is accepted as a rigid body and Newton-Euler laws of motion are used. The chosen state variables for this problem are $x = [u,\ v,\ w,\ p,\ q,\ r,\ \phi,\ \theta,\ \psi]$ where u, v, w denote linear velocities, p, q, r represent angular velocities and ϕ, θ, ψ indicate the Euler angles. The nonlinear equations of motion are given in equation (1) where, $V = [u\ v\ w]^T$ is the linear velocity vector of the system, $W = [p\ q\ r]^T$ is the angular velocity vector of the system, $F = [F_{X_b}\ F_{Y_b}\ F_{Z_b}]^T$ is the total force (aerodynamic and gravity) vector, and $M = [M_{X_b}\ M_{Y_b}\ M_{Z_b}]^T$ is the total aerodynamic moment vector while J is the inertia dyadic matrix of the rigid body.

$$F = m\left(\partial V/\partial t + W \times V\right), \quad M = \partial\left(J \cdot W\right)/\partial t + W \times \left(J \cdot W\right) \tag{1}$$

2.2. Control Actuator System (CAS)

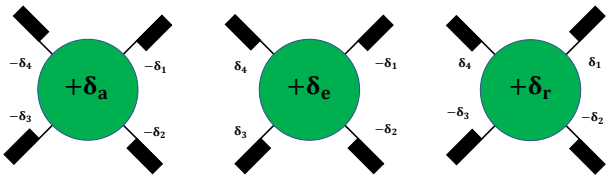

Figure 2: Positive control deflections

The control actuator system is used to steer the UAV. The rotational movements of the UAV are generally provided by aileron, elevator and rudder control surfaces. In the system, the control surfaces are provided by the various movements of four fins located in the tail section and working independently of each other.

In the reference geometry considered, the fins are positioned in an "×" shape with respect to the vehicle axes. In the case of the "×" configuration, the numbers of the fins and the positive direction of rotation of the leading edges are shown in figure 1b.

As a result, the rotation angles of different fins and the positive control surface effects they will create are shown in figure 2. When viewed from the rear and the vehicle center of gravity is in front of the fins, the positive elevator creates torques that lift the nose up, the positive rudder turns the nose to the right, and the positive aileron causes the right wing to turn down. The transition expression from the fin rotation angles to the control surface angles are given in equation (2).

$$\begin{bmatrix} \delta_a \\ \delta_e \\ \delta_r \end{bmatrix} = \frac{1}{4} \begin{bmatrix} -1 & -1 & -1 & -1 \\ -1 & -1 & 1 & 1 \\ 1 & -1 & -1 & 1 \end{bmatrix} \begin{bmatrix} \delta_1 \\ \delta_2 \\ \delta_3 \\ \delta_4 \end{bmatrix} \tag{2}$$

2.3. Linear Models

Before the controller design, the studied nonlinear system is linearized, by following the step given in [7], around 12000 meters and 0.95 Mach. The input vector u, state vector x and output vector y used in the linearization step are given in equation (3). δ_a, δ_e and δ_r in input vector represent the aileron, elevator and rudder deflection angles, respectively.

$$u = [\delta_a \ \delta_e \ \delta_r]^T, \quad x \equiv y = [u \ v \ w \ p \ q \ r \ \phi \ \theta \ \psi]^T \tag{3}$$

2.3.1. Roll Channel δ_a deflection angle is selected as the input variable for the roll channel, while the ϕ angle is selected as the output variable. The state variables of this channel are determined as angular velocity p and angle ϕ. The state-space representation of the roll channel is given in equation (4).

$$\begin{bmatrix} \dot{p} \\ \dot{\phi} \end{bmatrix} = \begin{bmatrix} -0.3448 & 0 \\ 1 & 0 \end{bmatrix} \begin{bmatrix} p \\ \phi \end{bmatrix} + \begin{bmatrix} 353.9702 \\ 0 \end{bmatrix} \delta_a, \quad y = \begin{bmatrix} 0 & 1 \end{bmatrix} \begin{bmatrix} p \\ \phi \end{bmatrix} \tag{4}$$

2.3.2. Pitch Channel δ_e deflection angle is selected as the input variable for the pitch channel, while the θ angle is selected as the output variable. The state variables of this channel are determined as linear velocity w, angular velocity q and angle θ. The state-space representation of the pitch channel is given in equation (5).

$$\begin{bmatrix} \dot{w} \\ \dot{q} \\ \dot{\theta} \end{bmatrix} = \begin{bmatrix} -0.4373 & 279.883 & 0.6843 \\ -0.2544 & -0.393 & 0 \\ 0 & 1 & 0 \end{bmatrix} \begin{bmatrix} w \\ q \\ \theta \end{bmatrix} + \begin{bmatrix} 13.3636 \\ 85.6141 \\ 0 \end{bmatrix} \delta_e, \quad y = \begin{bmatrix} 0 & 0 & 1 \end{bmatrix} \begin{bmatrix} w \\ q \\ \theta \end{bmatrix} \tag{5}$$

2.3.3. Yaw Channel δ_r deflection angle is selected as the input variable for the yaw channel, while the ψ angle is selected as the output variable. The state variables of this channel are determined as linear velocity v, angular velocity r and angle ψ. The state-space representation of the yaw channel is given in equation (6).

$$\begin{bmatrix} \dot{v} \\ \dot{r} \\ \dot{\psi} \end{bmatrix} = \begin{bmatrix} -0.1023 & -280.2497 & 0 \\ 0.2255 & -0.3834 & 0 \\ 0 & 1.0024 & 0 \end{bmatrix} \begin{bmatrix} v \\ r \\ \psi \end{bmatrix} + \begin{bmatrix} -16.3419 \\ 80.4806 \\ 0 \end{bmatrix} \delta_r, \quad y = \begin{bmatrix} 0 & 0 & 1 \end{bmatrix} \begin{bmatrix} v \\ r \\ \psi \end{bmatrix} \tag{6}$$

3. Controller design

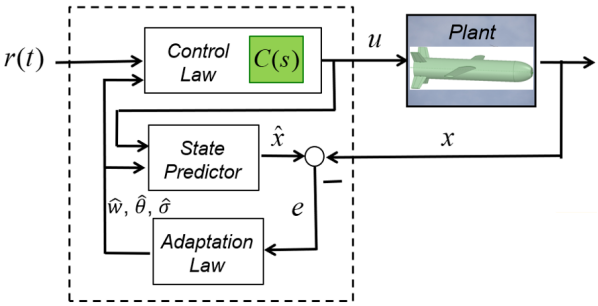

Figure 3: L_1 adaptive controller scheme.

The L_1 adaptive controller scheme is shown in figure 3. On the principle of model reference adaptive control (MRAC), the L_1 adaptive control is founded. By raising the adaptation gain in MRAC, the tracking error can be arbitrarily lowered; however, high adaptive gains result in large-gain feedback control, which can have negative effects on robustness and cause quick oscillations of the control signal [8].

By adding a low-pass filter to the control signal, the L_1 adaptive controller achieves its purpose of separating control from adaptation. In this way, unknown parameters can be adapted quickly

with a high adaptation gain. Examine the system in equation (7), where $x(t)$ is the system state vector, $u(t)$ is the control signal, $y(t)$ is the output, B, C are known system vectors, A_H is a known Hurwitz matrix defining the appropriate closed-loop dynamics, (A_H, B) is controllable pair, ω is an uncertain input gain, $\theta(t)$ is a vector of time varying unknowable parameters, and $\sigma(t)$ is disturbance of model.

$$\dot{x}(t) = A_H x(t) + B\left(\omega u(t) + \theta^T x(t) + \sigma(t)\right), \quad y(t) = C^T x(t) \tag{7}$$

With particular controller that is given in equation (8), u_{ideal}, $y(t)$ tracks step references with no steady-state error where $k_g = -1/(C^T A_H^{-1} B)$, and the uncertainties in equation (7) are entirely removed. This provides the perfect system in equation (9). The ideal controller, however, can not be used because it relies on the unknowable parameters ω, $\theta(t)$, and $\sigma(t)$. Consequently, adaptation is required to get the necessary control input $u(t)$.

$$u_{ideal}(t) = \frac{1}{\omega}\left(-\theta^T(t)x(t) - \sigma(t) + k_g r(t)\right) \tag{8}$$

$$\dot{x}_H(t) = A_H x_H(t) + B k_g r(t), \quad y_H(t) = C^T x_H(t) \tag{9}$$

There is a state predictor in equation (10) where $\hat{x}(t)$ is the predictor's state. The unknown parameters ω, $\theta(t)$, and $\sigma(t)$ have been substituted by their estimations in the predictor, which has the same structure as equation (7).

$$\dot{\hat{x}}(t) = A_H \hat{x}(t) + B\left(\hat{\omega} u(t) + \hat{\theta}^T(t)x(t) + \hat{\sigma}(t)\right), \quad \hat{y}(t) = C^T \hat{x}(t) \tag{10}$$

The adaptive law is provided in equation (11) for the unknown parameters where Proj is the projection operator and that is defined in equation (12) whereas Γ is the adaptation gain. The projection operator ensures that parameter estimates stay within predetermined limits [9]. Positive definite symmetric P solves the algebraic Lyapunov equation $A_H^T P + P A_H = -Q$ for arbitrary positive definite symmetric Q. The terms that have tilde sign in equation (11) represent errors between actual state values and their estimates.

$$\begin{aligned} &\dot{\hat{\omega}}(t) = \Gamma \,\mathrm{Proj}\left(\hat{\omega}(t), -\tilde{\mathbf{x}}^T(t)PBu(t)\right), \quad \dot{\hat{\theta}}(t) = \Gamma \,\mathrm{Proj}\left(\hat{\theta}(t), -\tilde{\mathbf{x}}^T(t)PB\left\|x(t)\right\|_\infty\right) \\ &\dot{\hat{\sigma}}(t) = \Gamma \,\mathrm{Proj}\left(\hat{\sigma}(t), -\tilde{\mathbf{x}}^T(t)PB\right) \end{aligned} \tag{11}$$

$$\mathrm{Proj}(X, Y) \triangleq \begin{cases} Y & \text{if } f(X) < 0, \\ Y & \text{if } f(X) \geq 0 \text{ and } \nabla f^\top Y \leq 0, \\ Y - \frac{\nabla f}{\|\nabla f\|}\left\langle \frac{\nabla f}{\|\nabla f\|}, Y \right\rangle f(X) & \text{if } f(X) \geq 0 \text{ and } \nabla f^\top Y > 0 \end{cases} \tag{12}$$

The primary design problem of the L_1 adaptive control theory is to create *C(s)* with the best balance of robustness and performance. That low pass filter's design is still a difficulty because there are no clear rules for how it should be constructed [8]. The Bode diagrams of the used low-pass filters are shown in figure 4.

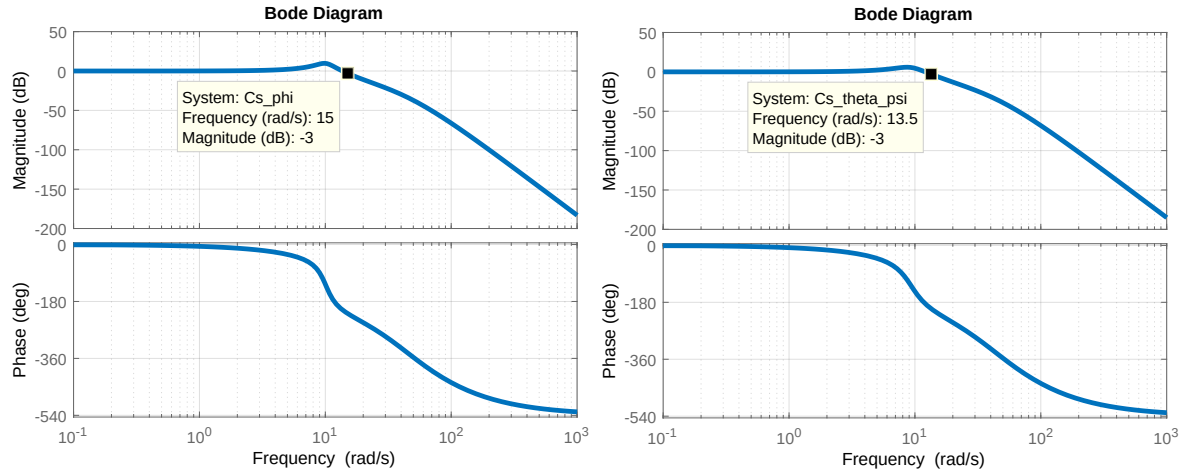

(a) Roll channel (b) Pitch and yaw channels

Figure 4: Bode diagrams of the low-pass filters

The state feedback vectors K_H, that were used with A and B matrices from linearization to get the desired system matrices ($A_H = A - BK_H^T$), are found with linear quadratic regulator (LQR). The Q and R matrices used to find the state feedback vectors of each channel and the found state feedback vectors are given in equation (13) where diag stands for diagonal matrix.

$$\begin{aligned} Q_{\text{roll}} &= \text{diag}(1, 50), \quad R_{\text{roll}} = 5, \quad K_{H_\phi} = \begin{bmatrix} 0.4658 & 3.1623 \end{bmatrix} \\ Q_{\text{pitch}} &= \text{diag}(0, 0, 30), \quad R_{\text{pitch}} = 2.5, \quad K_{H_\theta} = \begin{bmatrix} -0.0026 & 0.2479 & 3.4635 \end{bmatrix} \\ Q_{\text{yaw}} &= \text{diag}(0, 1, 30), \quad R_{\text{yaw}} = 1, \quad K_{H_\psi} = \begin{bmatrix} 0.0026 & 1.0527 & 5.4772 \end{bmatrix} \end{aligned} \tag{13}$$

The type of uncertainty taken into account in the simulations is provided in equation (14). The additional unmeasured error resulting from unmodeled actuator dynamics is given in equation (15).

$$\tilde{f}_x(t, x(t)) = A_\Delta(t)x(t) + \sigma(t), \quad \tilde{B}(t, x(t)) = B_\Delta(t) \tag{14}$$

$$\mu(t) = \omega u + \sigma_\mu(t) \tag{15}$$

The total modeling error can be expressed as in equation (16).

$$\begin{aligned} f(t, x(t)) &= BK_H^T(1 - \omega)x(t) + A_\Delta(t)x(t) + \sigma(t) \\ &+ (B + B_\Delta(t))\,\sigma_\mu(t) + B_\Delta(t)\left(\omega u - \omega K_H^T x(t)\right) \end{aligned} \tag{16}$$

The inequalities used to determine the limits of parameter estimates and adaptation gains are not included in this study. The steps for obtaining the inequalities can be found in the basic book [10], where the control theory used is discussed in detail. The system and input error matrices and the assumed maximum disturbance magnitudes used while determining the projection bounds are given in equation (17).

$$A_{\Delta_\phi} = \begin{bmatrix} 3 & 0 \\ 0 & 5 \end{bmatrix}, A_{\Delta_{\theta,\psi}} = \begin{bmatrix} 0 & 1 & 0 \\ 0 & 0 & 0 \\ 0 & 0 & 0 \end{bmatrix}, B_{\Delta_\phi} = \begin{bmatrix} 0 \\ 5 \end{bmatrix}, B_{\Delta_{\theta,\psi}} = \begin{bmatrix} 0.1 \\ 0.1 \\ 0.1 \end{bmatrix}, \sigma_{max_{\phi,\psi}} = \frac{\pi}{180}, \sigma_{max_\theta} = \frac{\pi}{18} \tag{17}$$

Unmatched uncertainty is the uncertainty that has different differential order with the control signal or in other words, can not meet the matching conditions [11]. The system structure accepted in this study can be given in equation (18). In this case, $f_m(.)$ represents the matched part of the unknowable uncertainties, whereas $B_{um}f_{um}(.)$ stands for the unmatched uncertainties and their definitions are given in equation (19).

$$\dot{x}(t) = A_H x(t) + B_m(\omega u(t) + f_m(t, x(t))) + B_{um} f_{um}(t, x(t)), \quad y(t) = C^T x(t) \tag{18}$$

$$[f_m(t, x(t)); f_{um}(t, x(t))] = [B_m \; B_{um}]^{-1} f(t, x(t)) \tag{19}$$

The bounds of matched model disturbances are chosen greater than equation (20) and the bounds of unmatched model disturbances are chosen greater than equation (21) where $B_m = B$, B_{um} is a matrix for unmatched inputs such that $B_m^T B_m = 0$ and $rank([B_m, B_{um}]) = n$ where n represents the state number of the related channel. The bounds of matched unknown parameters are chosen greater than sum of equation (22) and equation (23) while the bounds of unmatched unknown parameters are chosen greater than sum of equation (24) and equation (25).

$$\left\| \begin{bmatrix} 1 & 0_{1\times(n-1)} \\ 0_{(n-1)\times 1} & 0_{(n-1)\times(n-1)} \end{bmatrix} [B_m \; B_{um}]^{-1} \right\|_\infty \sigma_{\max} \tag{20}$$

$$\left\| \begin{bmatrix} 0 & 0_{1\times(n-1)} \\ 0_{(n-1)\times 1} & \mathbb{I}_{(n-1)\times(n-1)} \end{bmatrix} [B_m \; B_{um}]^{-1} \right\|_\infty \sigma_{\max} \tag{21}$$

$$\max_{A_\Delta(t)} \left\| \begin{bmatrix} 1 & 0_{1\times(n-1)} \\ 0_{(n-1)\times 1} & 0_{(n-1)\times(n-1)} \end{bmatrix} [B_m \; B_{um}]^{-1} A_\Delta \right\|_\infty \tag{22}$$

$$\max_{\tilde{B}(t)} \left\| \begin{bmatrix} 1 & 0_{1\times(n-1)} \\ 0_{(n-1)\times 1} & 0_{(n-1)\times(n-1)} \end{bmatrix} [B_m \; B_{um}]^{-1} B_\Delta K_H \right\|_\infty \tag{23}$$

$$\max_{A_\Delta(t)} \left\| \begin{bmatrix} 0 & 0_{1\times(n-1)} \\ 0_{(n-1)\times 1} & \mathbb{I}_{(n-1)\times(n-1)} \end{bmatrix} [B_m \; B_{um}]^{-1} A_\Delta \right\|_\infty \tag{24}$$

$$\max_{\tilde{B}(t)} \left\| \begin{bmatrix} 0 & 0_{1\times(n-1)} \\ 0_{(n-1)\times 1} & \mathbb{I}_{(n-1)\times(n-1)} \end{bmatrix} [B_m \; B_{um}]^{-1} B_\Delta K_H \right\|_\infty \tag{25}$$

The chosen bounds of disturbances (σ) and bounds of unknown parameters (θ) are given in equation (26) for each channel as matched and unmatched ones. The intervals of unknown input constants and the adaptation gains are selected as $w_{\phi,\theta,\psi} = [0.5, 2]$ and $\Gamma_{\phi,\theta,\psi} = 10000$ respectively.

$$\begin{aligned} &\sigma_{m_\phi} = 0.5, \sigma_{um_\phi} = 0.5175, \sigma_{m_\theta} = 1.0023, \sigma_{um_\theta} = 1.1994, \sigma_{m_\psi} = 1.0003, \sigma_{um_\psi} = 1.021 \\ &\theta_{m_\phi} = 0.5085, \theta_{um_\phi} = 23.64, \theta_{m_\theta} = 1.0067, \theta_{um_\theta} = 2.3594, \theta_{m_\psi} = 1.0086, \theta_{um_\psi} = 2.75 \end{aligned} \tag{26}$$

4. Results and Discussions

4.1. Linear System

For examining the operating performance of the channels under uncertainties, error matrices that containing sine waves are added to the system state matrices and reference trackings are examined. The amplitudes of the sine waves in the error matrices are determined by taking 50% of the relevant elements of the system state matrices. The frequencies of chirp sine waves varies from 0.15 Hz to 15 Hz in 20 seconds. The results in figure 5 show that adaptations to unknown parameters and reference trackings are achieved in all three channels.

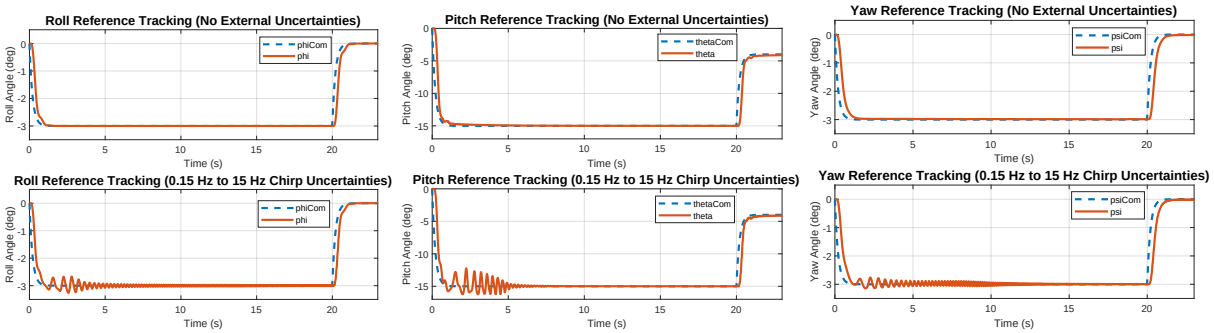

(a) Roll reference trackings (b) Pitch reference trackings (c) Yaw reference trackings

Figure 5: Linear systems' reference trackings

4.2. Nonlinear System

The simulation of the complete nonlinear UAV model is shown in this section. Without any fine-tuning, the controllers from the earlier parts are the ones utilized in the simulation. In addition to the nonlinearities incorporated into the UAV model, the simulation also includes measurement errors like tactical grade Inertial Measurement Unit (IMU) noises, disturbances like wind, and unmodeled dynamics. In the simulation, the UAV is launched from an altitude of 12000 meters with 0.95 Mach. A wind model that starts with 10 m/s velocity from South to North and decreases linearly in magnitude is chosen as a wind disturbance. In the IMU model, which is containing a three-axis accelerometer and three-axis gyroscope, the noise power is determined as 1e-6. The simulation is terminated when the UAV reached the ground. Reference trackings of Euler angles at some moments of the simulation and the graphs of state variables throughout the simulation are given in figure 6. The variations of angle of attack, side slip angle, altitude, wind, dynamic pressure and Mach number are shown in figure 7.

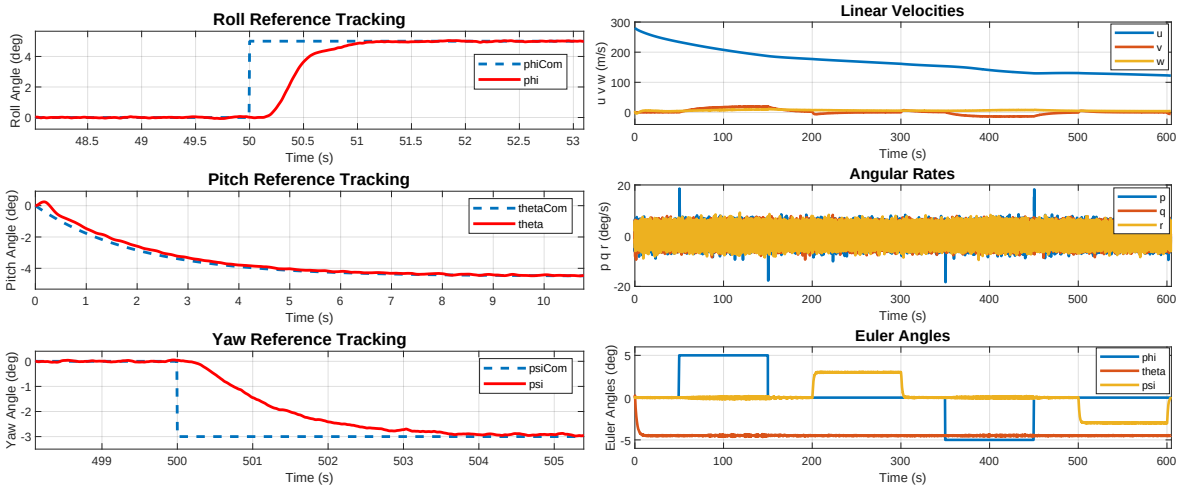

(a) Euler angles reference trackings (b) State variables

Figure 6: Reference trackings and state variables

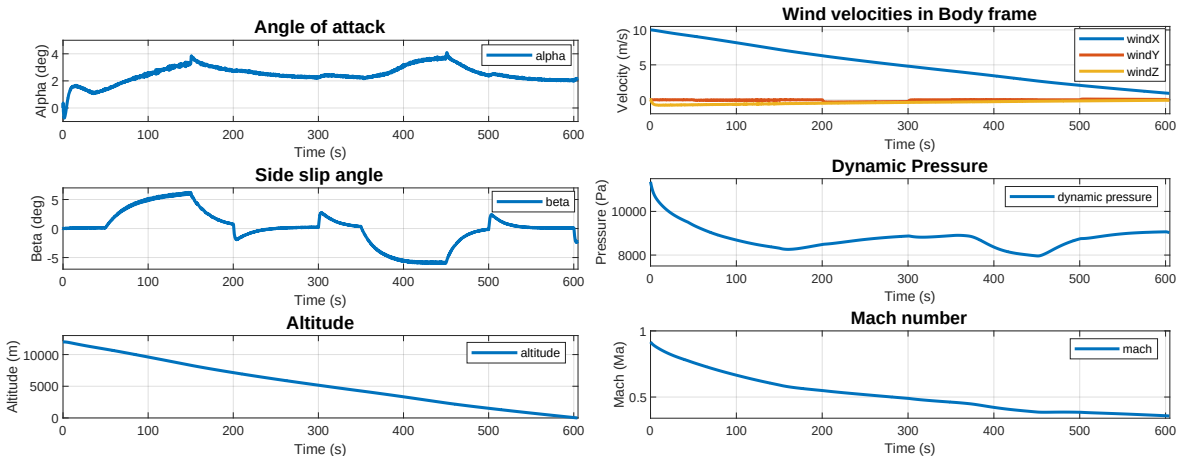

(a) Angle of attack, side-slip angle and altitude (b) Wind, dynamic pressure and Mach number

Figure 7: Angle of attack and side-slip, altitude, wind, dynamic pressure and Mach number

As a result of using the controller designed by considering a single trim point in the nonlinear system, all state variables are remained stable throughout the entire flight envelope. During the controller design phase, the actuator dynamics are considered as first-order low-pass filters. However, the actuator dynamics used in the nonlinear system are in the nonlinear second-order filter structure. Based on these, it can be concluded that the designed controller performed well under uncertainties, unmodeled dynamics, disturbances and noise.

5. Conclusion

A UAV's dynamics are continually changing while it is in the air. UAVs' relatively compact structures make them challenging to manage in noisy or disruptive environments, and the systems may even become unstable. For a fixed wing tail fin controlled UAV, the L_1 adaptive control structure is created. It is noted that good reference trackings are realized even when uncertainties are present and adaptations to unknown parameters are accomplished in all channels. Using the controller created by considering just one trim point in the nonlinear system, all state variables are remained stable over the course of the whole flight envelope. It has been observed that the L_1 adaptive controller performed well under disturbances, uncertainties and noise.

References

[1] Daponte P, De Vito L, Mazzilli G, Picariello F, Rapuano S and Riccio M 2015 *2015 IEEE Metrology for Aerospace (MetroAeroSpace)* (IEEE) pp 306–311

[2] Kürkçü B and Kasnakoğlu C 2018 *IEEE Transactions on Control Systems Technology* **27** 2622–2629

[3] Strub G, Theodoulis S, Gassmann V, Dobre S and Basset M 2018 *Journal of Guidance, Control, and Dynamics* **41** 461–475

[4] Baldi S, Sun D, Xia X, Zhou G and Liu D 2022 *IEEE Transactions on Aerospace and Electronic Systems*

[5] Albayrak M, Kürkçü B and Ayasun S 2022 *2022 IEEE 13th International Conference on Mechanical and Intelligent Manufacturing Technologies (ICMIMT)* (IEEE) pp 302–307

[6] Chai R, Tsourdos A, Gao H, Chai S and Xia Y 2022 *Automatica* **145** 110561

[7] Dong Y, Zhang Y and Ai J 2016 *Aerospace Science and Technology* **55** 292–306

[8] Holhjem Ø H 2012 L_1 *Adaptive Control of the Inner Control Loops of an F-16 Aircraft* Master's thesis Institutt for teknisk kybernetikk

[9] Lee K W and Singh S N 2012 *Acta Astronautica* **80** 24–35

[10] Hovakimyan N and Cao C 2010 L_1 *adaptive control theory: Guaranteed robustness with fast adaptation* (SIAM)

[11] Mittal S and Menq C H 1997 *IEEE/ASME Transactions on Mechatronics* **2** 268–280